Original Article
Feasibility of simultaneous PET/MR in diet-induced atherosclerotic minipig: a pilot study for translational imaging

Sune F Pedersen[1], Trine P Ludvigsen[2], Helle H Johannesen[3], Johan Löfgren[3], Rasmus S Ripa[1], Adam E Hansen[3], Anders J Ettrup[4], Berit Ø Christoffersen[5], Henrik D Pedersen[5], Lisbeth H Olsen[2], Liselotte Højgaard[1], Andreas Kjær[1]

[1]Cluster for Molecular Imaging, University of Copenhagen; Department of Clinical Physiology, Nuclear Medicine & PET, Rigshospitalet, University of Copenhagen, Copenhagen, Denmark; [2]Department of Veterinary Disease Biology, University of Copenhagen, Frederiksberg, Denmark; [3]Department of Clinical Physiology, Nuclear Medicine & PET, Rigshospitalet, University of Copenhagen, Copenhagen, Denmark; [4]Neurobiology Research Unit, Rigshospitalet, University of Copenhagen, Copenhagen, Denmark; [5]Diabetes Pharmacology, Novo Nordisk A/S, Måløv, Denmark

Abstract: Novel hybrid 18-fluoro-deoxy-D-glucose (^{18}F-FDG) based positron emission tomography (PET) and magnetic resonance imaging (MRI) has shown promise for characterization of atherosclerotic plaques clinically. The purpose of this study was to evaluate the method in a pre-clinical model of diet-induced atherosclerosis, based on the Göttingen minipig. Using ^{18}F-FDG PET/MRI the goal was to develop and create a new imaging method in an *in vivo* animal model for translational studies of atherosclerosis. We used a strategy of multisequence MRI for optimal anatomical imaging of the abdominal aortas of the pigs (n=4): T1-weighted turbo spin-echo (T1-TSE), T2-weighted turbo spin-echo (T2-TSE) and proton density imaging with and without fat saturation. ^{18}F-FDG PET emission data were collected from a single bed position of the abdominal aorta in 3D mode for either 10 (n=4) or 10 and 20 minutes (n=2) to measure glycolysis as given by standardized uptake values (SUV). Ex vivo *en face* evaluation of aortas from an atherosclerotic animal illustrated plaque distribution macroscopically, compared to a lean control animal. Although T2-TSE weighted imaging was most consistent, no one MRI sequence was preferable and superior to another for visualization and identification of the abdominal aorta. We found poor correlation between SUVs obtained from 10 and 20 minutes of reconstructed PET emission data. This can most likely be ascribed to intestinal movement. In conclusion multisequence MRI is recommended for optimal imaging of the abdominal aorta using MRI. Furthermore we found that 10 minutes of PET emission data seems adequate. This is the first study to demonstrate that the method of ^{18}F-FDG PET/MRI is feasible in minipig models of atherosclerosis, and therefore relevant in larger prospective studies. Perspectives of the method include correlation to *e.g.* aortic immunohistochemistry findings and a range of genomic and proteomic analyses.

Keywords: Atherosclerosis, novel model, Göttingen minipig, positron emission tomography, magnetic resonance imaging

Introduction

Atherosclerosis is a highly prevalent silent disease which usually lies dormant for decades until an advanced disease stage is reached through atheroma formation in the arteries [1]. At a later stage sudden disease onset such as stroke and myocardial infarction is precipitated by rupture of complicated atheroma (plaque) [2]. There is a need for non-invasive methods for atherosclerotic plaque detection to identify patients at risk. Positron emission tomography (PET) using 18-fluorodeoxyglucose (^{18}F-FDG) has been evaluated as a tool for detection of plaque inflammation and vulnerability by glycolytic activity in high-risk patients [3-5]. Furthermore clinical as well as pre-clinical studies indicate that crucial components in plaque composition can be characterized using magnetic resonance imaging (MRI) and that this cor-

related with histology [6, 7]. Recent work provided evidence that imaging is central in monitoring longitudinal drug effect; *e.g.* in studies evaluating the anti-inflammatory effect of statins in relation to atherosclerosis [8] or attenuated atherogenesis in the dal-PLAQUE study [9]. Pig models of atherosclerosis are well-described [10-12] and provide an important translational potential, also in relation to evaluation of drug effect [13]. Furthermore it has been established that porcine models develop accelerated atherosclerotic disease with pathological characteristics highly comparable to human atherosclerosis [10, 11]. Multi-modality imaging in a translational research model of human atherosclerosis potentiates improved diagnostics in relation to human disease as well as pre-clinical *in vivo* assessments *e.g.* in relation to early drug development (Ludvigsen TP *et al*; unpublished data).

Recently a whole-body integrated PET/MR system was introduced; the Siemens Biograph mMR, which allows simultaneous PET and MR imaging [14]. This integrated solution offers true isocentric acquisition of PET/MR signals thereby ameliorating the alignment of animals in a sequential PET/MR setup. In a recent vascular imaging study a head-to head comparison of 18F-FDG PET/MR and PET/CT was performed. Although a small but significant systematic bias towards lower standardized uptake values (SUVs) was found for the PET/MR system compared to PET/CT, it was concluded that vascular imaging by PET/MR was feasible [15].

The aim of this pilot study was to develop and evaluate 18F-FDG PET/MR-imaging of the abdominal aorta in normal and atherosclerotic Göttingen minipigs.

Materials and methods

Animals and study design

Animals included in the study (n=4) were male castrated Göttingen minipigs (Ellegaard Göttingen Minipigs A/S, Dalmose, Denmark), housed at University of Copenhagen, Denmark. Three of the animals were fed a high-fat, high-cholesterol diet, containing 1 or 2% cholesterol (5B4L,TestDiet®, St. Louis, Missouri, US) and one lean control animal was fed standard mini-pig diet (Mini-pig diet, Special diet services, Essex, UK) (Ludvigsen TP *et al*; unpublished

data). The examined animals were part of other experiments, not further described here. Animals had IV access established in the auricular or jugular vein, either at the day of PET/MR acquisition or within one week preceding the imaging procedures. Animals were fasted overnight and anesthetized prior to the imaging procedure using an IM dose of a mixture of tiletamin and zolazepam (0.81 mg/kg of both tiletamin and zolazepam (Zoletil 50 Vet, ChemVet, Silkeborg, Denmark)), with added ketamine (0.81 mg/kg) (Ketaminol Vet (100 mg/ml), Intervet, Skovlunde,Denmark), xylazine (0.84 mg/kg) (Rompun Vet (20 mg/ml) Bayer, Lyngby, Denmark) and buthorphanol (0.16 mg/kg) (Torbugesic (10 mg/ml) Scanvet, Fredensborg, Denmark). Animals were maintained in anesthesia by intramuscular dosing of 1/3 of the induction dose every 45-60 minutes throughout the procedures. In three animals, a colostomy bag (Coloplast®) was placed surrounding the preputium to avoid urine spill and in one animal, a temporary transcutaneous suprapubic catheter was inserted [16]. Animals were intubated and breathing spontaneously with O_2 supplement during imaging procedures. Exclusion criteria were fever and generalized malaise immediately prior to experimental procedures as well as blood glucose >200 mg/dL (11.1 mmol/L) at the time of 18F-FDG administration [17]. The study was approved by the Animal Experiments Inspectorate, Ministry of Justice, Denmark.

18F-FDG PET imaging

18F-FDG PET images were acquired using a hybrid PET/MR scanner (Biograph mMR, Siemens AG, Erlangen, Germany). Immediately preceding injection of 18F-FDG (252-424 MBq) blood glucose was measured, see **Table 1**. Subsequent to 18F-FDG administration the animals were placed in the scanner in the lateral position for PET/MR imaging. To allow distribution and uptake of 18F-FDG, PET acquisition was started one hour post-injection. Emission data were collected from a single bed position of the abdominal aorta for 10 minutes in 3D mode for all animals. Additionally, animals in substudy B had emission data collected for 20 minutes in 3D mode for comparison of scanning times. Reconstruction of PET images was performed on the mMR console using vendor supplied attenuation correction (Dixon-based) and 3D OSEM with 6 iterations, 21 subsets,

Table 1. Background characteristics of animals in the study

Sub-study	Animal ID	Weight (kg)	Age (weeks)	Blood glucose (mmol/L)*	Group	Note	Atherogenic diet time	TC mmol/L#	^{18}F-FDG/ MBq
A	1	60	55	6.3	Obese		41 weeks	31.4	398
A	2	27	54	7	Lean control			3.8	424
B	3	27	38	7.7	Obese	Statin treated	12 weeks	13.8	396
B	4	25	38	10.7	Obese	Statin treated	12 weeks	7.1	252
						Transcutaneous urethral catheter			

*Measured immediately preceding injection of ^{18}F-FDG. #Evaluated one week ± examination time. ^{18}F-FDG = ^{18}F-fluorodeoxyglucose, MBq = Megabequerel, TC = Total cholesterol.

Table 2. ^{18}F-FDG-uptake: Results and descriptive statistics

Animal	Diet	Mean SUV$_{mean}$*	Mean SUV$_{max}$*	n (slices)
1	High-fat diet	0.83 ± 0.06	1.43 ± 0.09	6
2	Normal chow	0.95 ± 0.07	1.18 ± 0.07	6
3	High-fat diet	0.99 ± 0.03	1.37 ± 0.08	4
4	High-fat diet	0.47 ± 0.04	0.89 ± 0.04	5

*Mean ± SEM. SUV = Standardized uptake value.

image matrix 512, a zoom factor of 2 and 2 mm Gaussian post-reconstruction filter. This resulted in a reconstructed voxel size of 0.7 × 0.7 × 2.0 mm³.

MR imaging

MR acquisition was initiated as soon as the animals were placed in the scanner and continued throughout the PET procedure. The segment of interest in the abdominal aorta was identified on a coronal T1-weighted turbo spin-echo (T1-TSE) sequence. In order to evaluate optimal sequencing for high resolution anatomical imaging, two animals (1 and 2) received axial T1-TSE, T2-weighted turbo spin echo (T2-TSE) and proton density weighted imaging without fat saturation. Two other animals (3 and 4) received T1-TSE, T2-TSE and proton density weighted imaging with fat saturation. All sequences were triggered by electrocardiogram: an ECG-unit was integrated in the MR-modality, and electrodes tape-fixated on the thorax of the animals for ECG trigging of MR sequences. Sufficient quality of the ECG for recognition of the R-segment was assured prior to the scan. Receiving-coils were placed at the flank of the animals in the abdominal region.

PET quantification

PET and MR images were automatically co-registered using the mMR console. For image analysis of *in vivo* PET data, regions of interest (ROIs) were drawn in free hand on corresponding axial MR images. The ROIs were drawn to encompass the entire vessel wall and lumen starting from the left renal artery and proceeding caudally towards the aortic bifurcature yielding consecutive transaxial slices of 2 mm thickness using Mirada software (Mirada Medical, Oxford, UK). Four to six slices were measured depending on the size of the animal. Quantification of ROIs was performed using the SUV of which mean and maximum SUV values were obtained (SUV$_{mean}$, SUV$_{max}$).

En face processing of vessels

Subsequent to sacrifice of the animal, the aorta was opened ventrally, excised above the *truncus coeliacus*, pinned out, immersion fixated in 10% buffered formalin for minimum 24 hours, and stained using Sudan IV for visualization of lipids and plaque (**Figure 5**).

Statistical analysis

Data are presented either as raw data plotted with an inserted line representing the median value or as mean ± SEM. Analyses were performed using SPSS 20 (IBM Corporation, Armonk, New York, USA) and graphical illustrations in Graphpad Prism 5 (Graphpad software Inc, La Jolla, CA, US). Normal distribution assumptions were tested using the Kolmogorov-Smirnov test. To compare *in vivo* PET emission times (10 and 20 minutes) from the same animal, a two-tailed paired t-test was applied with $P < 0.05$ considered statistical significant.

Results

In **Table 1**, background characteristics on animals included in the study is presented and results from the ^{18}F-FDG PET is seen in **Table 2**.
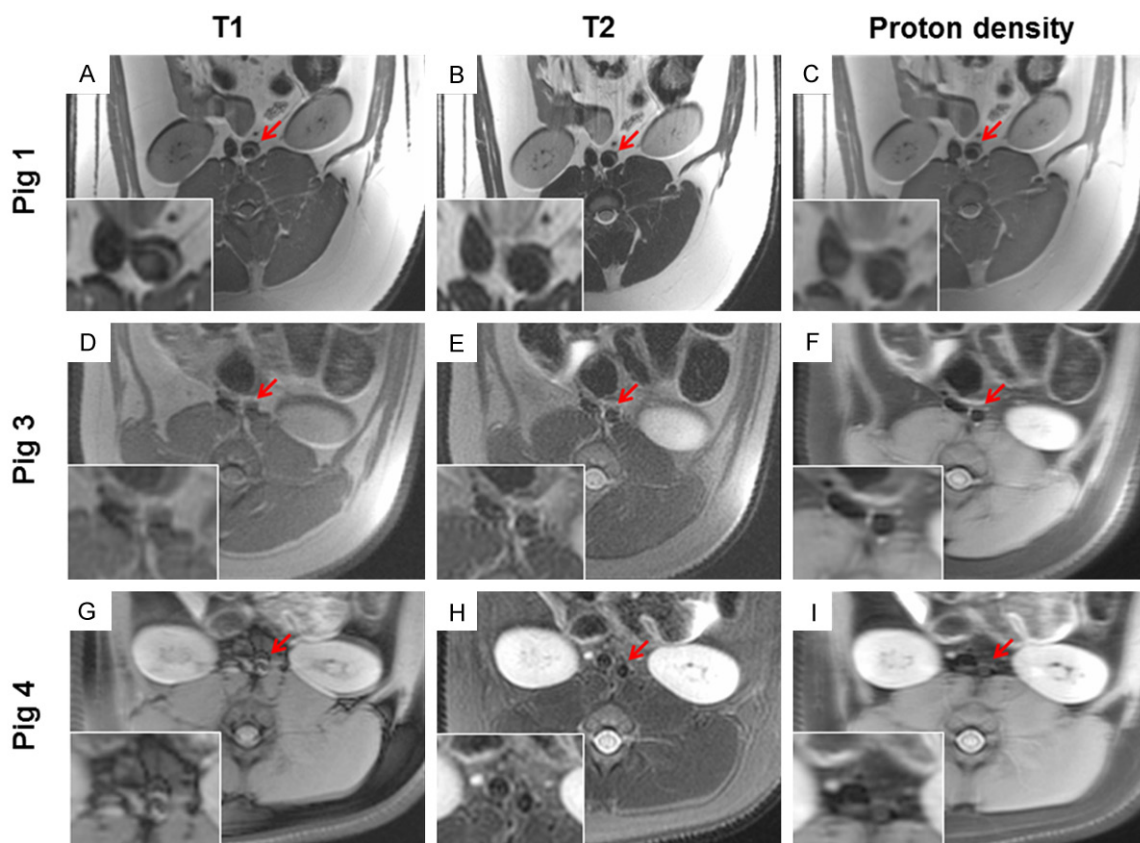
Figure 1. Representative *in vivo* magnetic resonance imaging of *a. abdominalis* in 3 different pigs illustrating how choice of MRI-sequence affects image quality. In this regard pig 2 were identical in quality to pig 1 and was omitted from the figure. Left panels are T1-weighted images, middle panels are T2-weighted images and right panels are proton density weighted images. Image A to C are without fat saturation and image D to I is with fat saturation. (A-C) Pig 1 imaged after 41 weeks of high-fat diet, (D-F) pig 3 imaged after 12 weeks of high-fat diet and statin treatment and finally (G-I) pig 4 imaged after 12 weeks of high-fat diet and statin treatment. Red arrows indicate the abdominal aorta and inserted in the bottom left corner of each image a magnified view is provided.

In **Figure 1**, representative MRI images are illustrated whereas **Figure 2** shows combined PET/MR imaging and ROI placement. In **Figures 3** and **4**, results from SUV_{mean} and SUV_{max} are plotted, with data presented with lines at median values.

MR imaging of abdominal aorta

MR imaging was performed prior to and throughout the PET procedure for visualization of the abdominal aorta which subsequently was identified on transaxial slices in T1-, T2 and proton density-weighted images, as shown in **Figure 1**. The image quality was variable depending on both individual factors as well as the applied image sequence. Image acquisitions without fat-saturation are illustrated in **Figure 1A-C**, whereas **Figure 1D-I** illustrate acquisitions using fat-saturation. Nonfat-saturated images display a characteristic cres-

cent-shaped artifact particularly dominant at the ventral part of each kidney as well as vessel, seen in the magnified insert (**Figure 1A-C**). From visual inspection, T2- and proton density-weighted images for pig 1 (**Figure 1B** and **1C**) and 3 (**Figure 1E** and **1F**) are comparable and of better quality than T1-weighted images (**Figure 1A** and **1D**) from both animals. However for pig 4 (**Figure 1G-I**) only the T2-weighted image (**Figure 1H**) was of sufficient quality to identify the abdominal aorta. Apparently, the crescent-shaped artifacts are less pronounced when using fat-saturation; however ROIs were drawn on the most satisfactory sequence as illustrated in **Figure 2**.

Detection of glycolytic activity in the abdominal aorta by 18F-FDG PET

18F-FDG PET scans demonstrated glycolytic activity, expressed as SUV-values, localized to
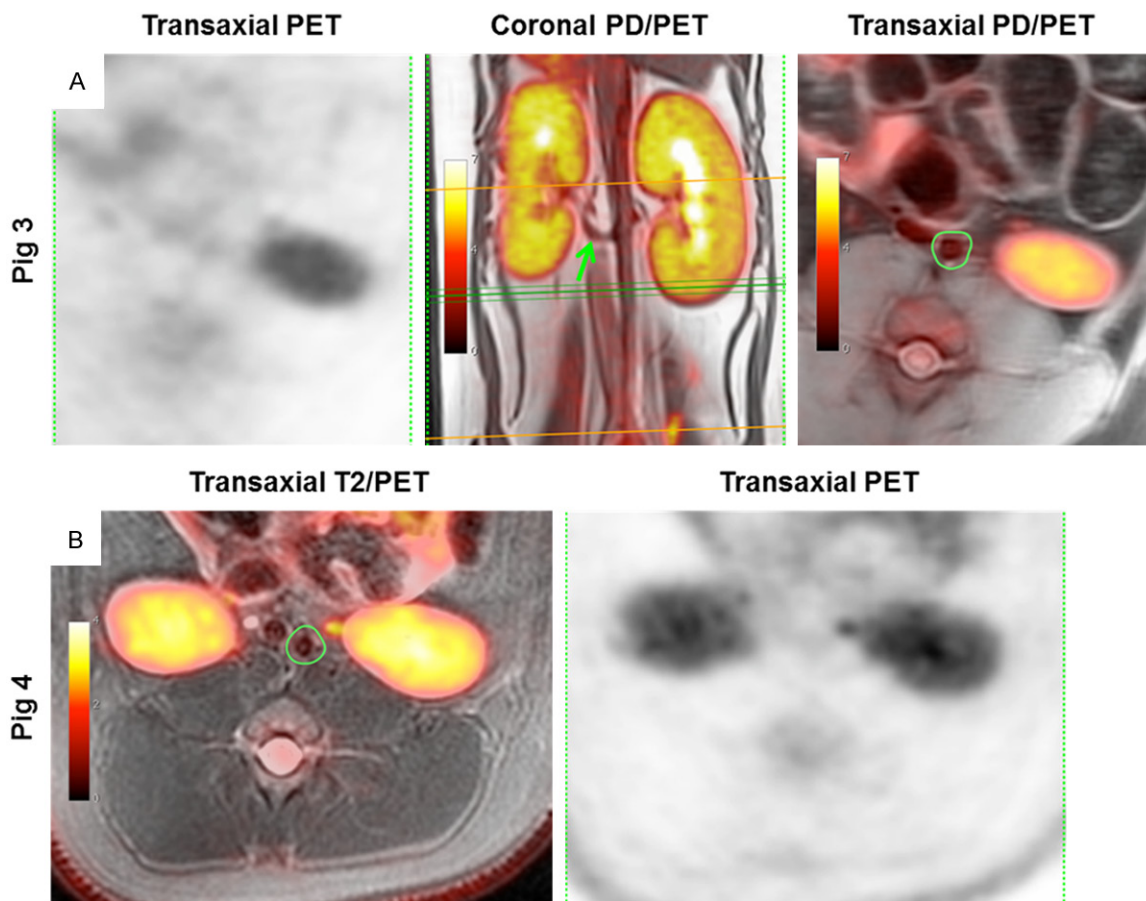
Figure 2. Representative *in vivo* combined PET/MR and PET images of *a. abdominalis* illustrating ^{18}F-FDG uptake (A) Left to right: ^{18}F-FDG PET and proton density (PD) weighted images combined with PET; the coronal projection shows *a. renalis sinistra* fusing with *a. abdominalis* (green arrow) and the green lines are the image plane for the transaxial slice seen far right with the ROI drawn to encompass lumen and wall of the vessel of pig 3. (B) T2-weighted image combined with PET; transaxial projection with ROI as in figure A (far right) of pig 4. Intensity bars indicate SUV-values. ^{18}F-FDG = 18-fluorodeoxyglucose, PET = Positron emission tomography, ROIs = Regions of interest, SUV = Standardized uptake value.

the abdominal aorta of the animals fed an atherogenic diet as well as the animals fed normal chow (see **Table 2**). Importantly, ^{18}F-FDG uptake was seen to be heterogeneously distributed in the abdominal aorta as determined transaxially on a slice by slice basis (see **Figure 3**). Furthermore **Figure 3** shows that catheterization, and thereby bladder voiding, looks to influence the SUV values obtained in the *a. abdominalis* region. We also calculated coefficients of variation (CV%) of the obtained SUV-values from both 10 and 20 minutes of PET emission data from the animals in substudy B. Pig 3 showed SUV$_{mean}$: (10 minutes; CV=6.5% and 20 minutes; CV=6.6%) and SUV$_{max}$: (10 minutes; CV=11.7% and 20 minutes; CV=6.3%), whereas pig 4 showed SUV$_{mean}$: (10 minutes; CV=20.6% and 20 minutes; CV=14.1%) and SUV$_{max}$: (10

minutes; CV=42.9% and 20 minutes; CV= 55.0%). Finally the SUV-values from the associated 10 and 20 minutes of PET emission data reconstructed dataset were illustrated and tested using a two-tailed paired t-test for comparison of the agreement between short and long reconstruction time. Except from the first animal (p=0.2034; see **Figure 4A**) there was a tendency of poor agreement of SUV-values between shorter (10 minutes) versus longer (20 minutes) emission time (p<0.05; **Figure 4B**, p=0.0712; **Figure 4C** and p=0.0944; **Figure 4D**).

Discussion

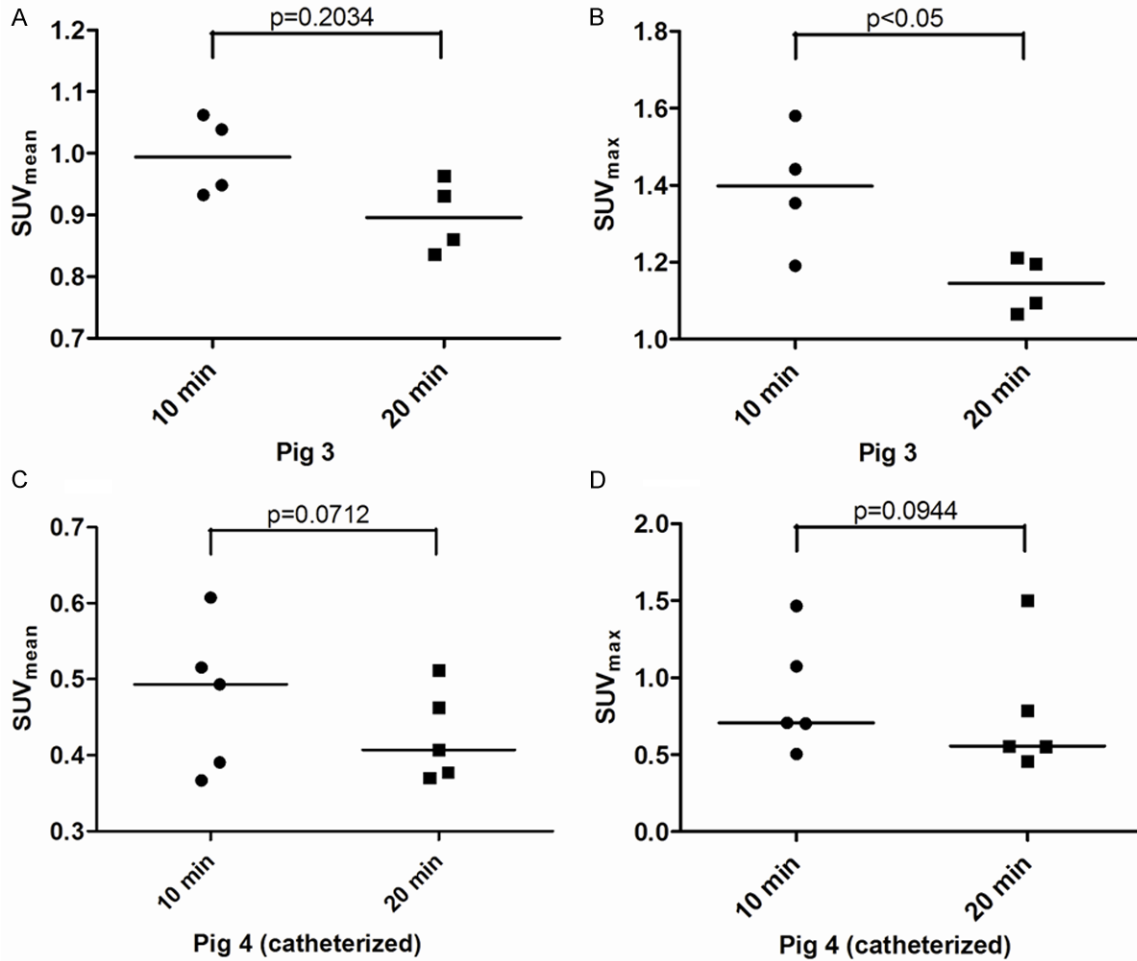PET/MR imaging in Göttingen minipigs can reveal atherosclerosis and a new method for in
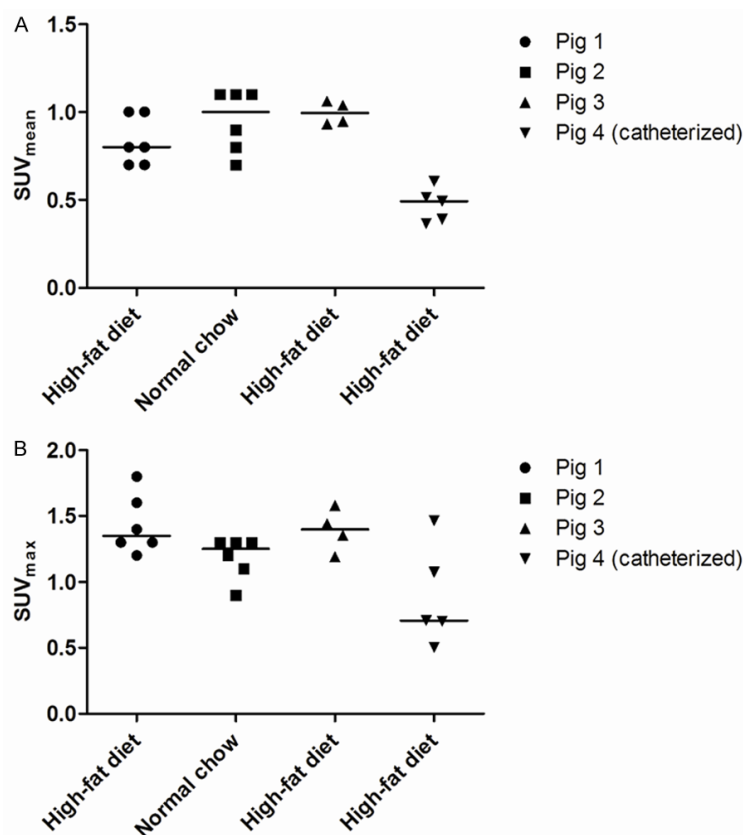
Figure 3. ^{18}F-FDG uptake in consecutive 2 mm thick transaxial voxels from ROIs of *aorta abdominalis* caudal to *arteria renalis sinistra* of pigs either on high-fat diet (n=3) or receiving normal chow (n=1). PET scans were obtained either without bladder voiding or catheterized (pig 4). A: ^{18}F-FDG uptake measured as mean standardized uptake value (SUV$_{mean}$). B: ^{18}F-FDG uptake measured as maximum standardized uptake value (SUV$_{max}$). Lines indicate median value. ^{18}F-FDG = 18-fluorodeoxyglucose, PET = Positron emission tomography, ROIs = Regions of interest, SUV = Standardized uptake value. Catheterized = a transcutaneous catheter was placed in the bladder of the animal.

mens [5]. Pre-clinically the feasibility of ^{18}F-FDG PET for evaluation of atherosclerosis *in vivo* has been confirmed using both mouse [22, 23] and rabbit models [6, 24, 25]. Important limitations of these studies include the limited size and biological similarity of the cardiovascular systems of mice and rabbits with that of humans, as well as the limited possibilities for repeated imaging based evaluations. By using a Göttingen minipig model of atherosclerosis, consecutive repetitive PET imaging can be performed to attain valuable information on disease status, progression and response to therapeutical intervention. When evaluating the minipig model we learned that lesions are rare in thoracic aorta and patchy at best in the arcus, whereas the abdominal aorta is globally affected. Generally the pig abdominal aorta including bifurcations is more susceptible to develop atherosclerosis, compared to the thoracic aorta, which is comparable to human disease [11]. Therefore the abdominal aorta was the natural choice for the purpose of this investigation.

PET has been applied in cardiovascular research because it offers quantifiable non-invasive imaging of cellular and molecular targets with an unsurpassed sensitivity both clinically and pre-clinically. ^{18}F-FDG is the most widely available validated PET tracer in nuclear medicine, and it is extensively used in the clinic [26]. In this pilot study we have demonstrated the feasibility of *in vivo* ^{18}F-FDG PET/MR imaging for anatomical visualization and measurement of glycolysis in the abdominal aorta in a Göttingen minipig model of atherosclerosis. We observed that the non-fat-saturated MRI sequences of the abdominal aorta displayed marked crescent-shaped artefacts of the vessel wall, as well as at the delineation of the kidneys in T1, T2 and PD-weighted imaging. When subsequently applying fat-saturation, the artefacts became

vivo assessment of atherosclerosis in an highly relevant translational model has hereby been developed. Increased glycolysis in the wall of arteries is a recognized feature primarily ascribed to activated macrophages in clinical as well as pre-clinical atherosclerosis, and has been demonstrated extensively using both *in vitro* models as well as *in vivo* techniques. Cell studies of atherosclerosis demonstrated how macrophage activation as well as hypoxia is responsible for an increase in glycolysis measured by uptake of actual ^{18}F-FDG or an *in vitro* analogue to ^{18}F-FDG; tritiated 2-deoxy-D-glucose (^{3}H-2dG) [18, 19]. Clinically assessment of glycolysis has been used to study atherosclerosis *in vivo* using ^{18}F-FDG PET [5, 20, 21] supported by autoradiography of clinical speci-

Figure 4. ^{18}F-FDG uptake calculated from consecutive 2 mm thick transaxial voxels from ROIs of *aorta abdominalis* caudal to *arteria renalis sinistra* from pigs 3 (A and B, SUV$_{mean}$/SUV$_{max}$) and 4 (C and D, SUV$_{mean}$/SUV$_{max}$) with reconstruction of either 10 or 20 minutes of PET emission data. PET scans were obtained either without bladder voiding or catheterized (pig 4). Data was tested using a two-tailed paired t-test. ^{18}F-FDG = 18-fluorodeoxyglucose, PET = Positron emission tomography, ROIs = Regions of interest, SUV = Standardized uptake value. Lines indicate median values.

less pronounced, however image contrast now declined compared to that of the non-fat-saturated images. In addition, the consistency of image quality in terms of identification of the abdominal aorta varied somewhat between animals even when using the same MR-sequence. Overall the most consistent images were obtained using T2-weighted sequences.

The *in vivo* detection of glycolysis displayed normal physiological uptake of ^{18}F-FDG in the intestinal wall, as well as excretion by the kidneys in every animal. ^{18}F-FDG uptake in consecutive segments of the abdominal aorta demonstrated a heterogeneous pattern of glycolysis along the course of the vessel which is in agreement with previous reports [3, 27].

Furthermore we observed that SUV values were less pronounced in the abdominal aorta of the animal with the transcutaneous bladder catheter. This suggests that bladder voiding is essential, as the close proximity of the vessel to the bladder means the ^{18}F-FDG signal from the vessel could be influenced by spillover from the bladder [28]. Finally, when comparing reconstruction of 10 and 20 minutes of PET emission data we found some inconsistency in the obtained SUV values. However, intestinal motility as well as displacement of the abdominal aorta even with slight increases in bladder volume (not applicable to the catheterized animal) during the additional 10 minutes of PET acquisition could cause image matrix shift. This phenomenon particularly affects small structures,
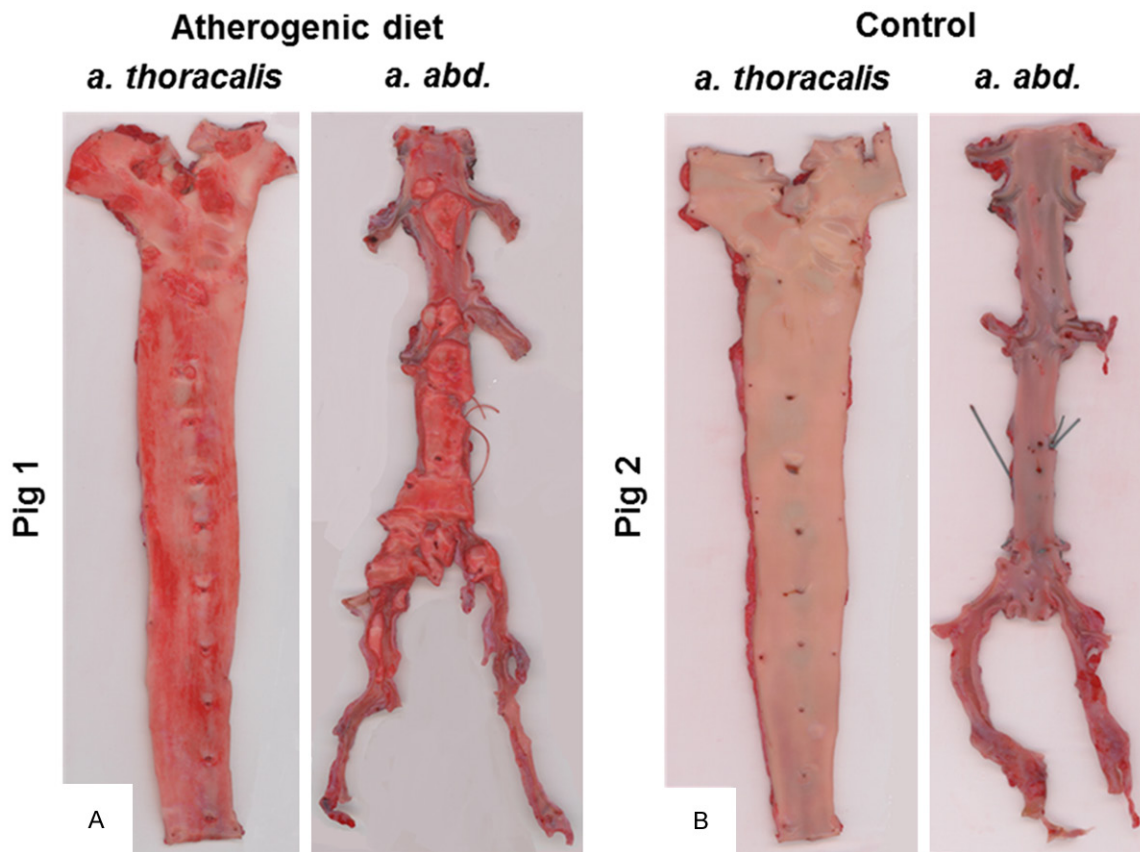
Figure 5. Aortas *ex vivo* from the obese atherogenic diet-fed pig (A, pig 1) and a lean pig from the control group (B, pig 2). After removal, the entire aorta was opened ventrally, excised above the *truncus coeliacus*, pinned out, immersion fixated in 10% buffered formalin for minimum 24 hours, and stained with a lipophilic staining (Sudan IV). Besides overall increased lipophilic staining in the obese animal (red lesions) (A), raised lesions are observed especially in the abdominal part of the aorta (right segment on each picture).

resulting in change in SUV values of a magnitude comparable to what we are observing in this study [29]. Use of antispasmodic (*e.g.* butylscopolamine) to avoid intestinal motility was deliberately deselected in these studies after observing tachycardia in anesthetized pigs upon intravenous administration in unrelated experiments.

Endogenous blood glucose levels are important for standardization of ^{18}F-FDG PET imaging [29]. Therefore animal inclusion should follow pre-determined criteria prior to ^{18}F-FDG administration subject to exclusion on non-compliance. Xylazine, one of the added components in the applied anesthetic is an α_2-adrenergic receptor agonists known to induce transient hypoinsulinemia in several species [30-32]. This could lead to an undesired increase in blood glucose level which, theoretically, could be proportional to the time the animal needs to

be anesthetized. When considering the body of work using ^{18}F-FDG PET data with a post-injection scanning time of one hour, this could be considered acceptable. However a very recent clinical study concluded that as much as 2.5 hours of ^{18}F-FDG distribution prior to the PET procedure was desirable, as was a blood glucose target of ≤7.0 mmol/L [33]. Taken together, either an alternative strategy for anesthesia should be pursued, or additional studies should be performed to determine maximum acceptable tracer distribution time using the current anesthesia regime. This should be in regard to the effect of xylazine on blood glucose levels, as well as to what can be considered acceptable in regard to animal welfare.

The recent clinical dal-PLAQUE study used ^{18}F-FDG PET to determine that treatment with a modulator of cholesteryl ester transfer protein (dalcetrapib) led to a significant reduction in

18F-FDG uptake in the most-diseased-segment of the carotid arteries of patients receiving dalcetrapib when compared to a placebo group [9]. Another recent clinical study demonstrated how a protein kinase inhibitor reduced vascular inflammation in the most inflamed vascular regions using 18F-FDG PET as a primary endpoint [34]. Accordingly PET seems to be a very promising technique for monitoring noninvasive *in vivo* longitudinal developments in disease in response to any desired interventional regime. However further studies are warranted prior to a larger prospective setup.

This pilot study was primarily focused on the feasibility of PET/MR imaging of a minipig model of atherosclerosis using a methodological and practical approach. Therefore, the included animals came from less well defined groups than would be the case in an actual prospective setup which can be observed from consulting the background animal characteristics (**Table 1**). This means that any deductions to anything other than the observed imaging parameters are at readers' discretion.

Secondly; statin treatment has been observed clinically as well as pre-clinically to cause reduction in plaque 18F-FDG uptake [27, 35] and even plaque regression, which could have influenced our PET/MR observations in substudy B by an unknown magnitude. Thirdly; although prescan blood glucose levels were considered in accordance with clinical criteria, they varied substantially to that of the natural levels of the minipigs and therefore 18F-FDG PET data should be interpreted with care.

Conclusion

This study is the first to demonstrate the feasibility of a novel imaging approach in relation to atherosclerosis using combined PET/MR in a Göttingen minipig model. We found that multi-sequence MR imaging should be recommended for optimal visualization and identification of the abdominal aorta. Furthermore collection and reconstruction of 10 minutes of PET emission data should be sufficient for larger prospective studies, however further studies including more animals are warranted. This model implies that lesions found with PET/MR can be correlated to histology, immunohistochemistry, gene-expression and other relevant markers for selected relevant artery regions.

We recommend that future prospective studies should include more animals in well-defined groups, multimodal MR-imaging and a minimum of 10 minutes of PET emission data collection.

Disclosure of conflict of interest

None.

Address correspondence to: Dr. Andreas Kjaer, Department of Clinical Physiology, Nuclear Medicine & PET and Cluster for Molecular Imaging, Rigshospitalet & University of Copenhagen, Blegdamsvej 9, DK-2100 Copenhagen, Denmark. E-mail: akjaer@sund.ku.dk

References

[1] Ross R. Atherosclerosis--an inflammatory disease. N Engl J Med 1999; 340: 115-126.
[2] Falk E, Shah PK and Fuster V. Coronary plaque disruption. Circulation 1995; 92: 657-671.
[3] Pedersen SF, Graebe M, Fisker Hag AM, Hojgaard L, Sillesen H and Kjaer A. Gene expression and 18FDG uptake in atherosclerotic carotid plaques. Nucl Med Commun 2010; 31: 423-429.
[4] Graebe M, Pedersen SF, Borgwardt L, Hojgaard L, Sillesen H and Kjaer A. Molecular pathology in vulnerable carotid plaques: correlation with [18]-fluorodeoxyglucose positron emission tomography (FDG-PET). Eur J Vasc Endovasc Surg 2009; 37: 714-721.
[5] Rudd JH, Warburton EA, Fryer TD, Jones HA, Clark JC, Antoun N, Johnstrom P, Davenport AP, Kirkpatrick PJ, Arch BN, Pickard JD and Weissberg PL. Imaging atherosclerotic plaque inflammation with [18F]-fluorodeoxyglucose po-

sitron emission tomography. Circulation 2002; 105: 2708-2711.

[6] Millon A, Dickson SD, Klink A, Izquierdo-Garcia D, Bini J, Lancelot E, Ballet S, Robert P, Mateo de CJ, Corot C and Fayad ZA. Monitoring plaque inflammation in atherosclerotic rabbits with an iron oxide (P904) and (18)F-FDG using a combined PET/MR scanner. Atherosclerosis 2013; 228: 339-345.

[7] Cai JM, Hatsukami TS, Ferguson MS, Small R, Polissar NL and Yuan C. Classification of human carotid atherosclerotic lesions with in vivo multicontrast magnetic resonance imaging. Circulation 2002; 106: 1368-1373.

[8] Tahara N, Kai H, Ishibashi M, Nakaura H, Kaida H, Baba K, Hayabuchi N and Imaizumi T. Simvastatin attenuates plaque inflammation: evaluation by fluorodeoxyglucose positron emission tomography. J Am Coll Cardiol 2006; 48: 1825-1831.

[9] Fayad ZA, Mani V, Woodward M, Kallend D, Abt M, Burgess T, Fuster V, Ballantyne CM, Stein EA, Tardif JC, Rudd JH, Farkouh ME and Tawakol A. Safety and efficacy of dalcetrapib on atherosclerotic disease using novel non-invasive multimodality imaging (dal-PLAQUE): a randomised clinical trial. Lancet 2011; 378: 1547-1559.

[10] Granada JF, Kaluza GL, Wilensky RL, Biedermann BC, Schwartz RS and Falk E. Porcine models of coronary atherosclerosis and vulnerable plaque for imaging and interventional research. EuroIntervention 2009; 5: 140-148.

[11] Hamamdzic D and Wilensky RL. Porcine models of accelerated coronary atherosclerosis: role of diabetes mellitus and hypercholesterolemia. J Diabetes Res 2013; 2013: 761415.

[12] Sturek M. Ca2+ regulatory mechanisms of exercise protection against coronary artery disease in metabolic syndrome and diabetes. J Appl Physiol (1985) 2011; 111: 573-586.

[13] Wilensky RL, Shi Y, Mohler ER, III, Hamamdzic D, Burgert ME, Li J, Postle A, Fenning RS, Bollinger JG, Hoffman BE, Pelchovitz DJ, Yang J, Mirabile RC, Webb CL, Zhang L, Zhang P, Gelb MH, Walker MC, Zalewski A and Macphee CH. Inhibition of lipoprotein-associated phospholipase A2 reduces complex coronary atherosclerotic plaque development. Nat Med 2008; 14: 1059-1066.

[14] Delso G, Furst S, Jakoby B, Ladebeck R, Ganter C, Nekolla SG, Schwaiger M and Ziegler SI. Performance measurements of the Siemens mMR integrated whole-body PET/MR scanner. J Nucl Med 2011; 52: 1914-1922.

[15] Ripa RS, Knudsen A, Hag AM, Lebech AM, Loft A, Keller SH, Hansen AE, von BE, Hojgaard L and Kjaer A. Feasibility of simultaneous PET/MR of the carotid artery: first clinical experience and comparison to PET/CT. Am J Nucl Med Mol Imaging 2013; 3: 361-371.

[16] Swindle MM. Urinary system and adrenal glands. Second edition. 2007. pp. 157-172.

[17] Adams MC, Turkington TG, Wilson JM and Wong TZ. A systematic review of the factors affecting accuracy of SUV measurements. AJR Am J Roentgenol 2010; 195: 310-320.

[18] Deichen JT, Prante O, Gack M, Schmiedehausen K and Kuwert T. Uptake of [18F]fluorodeoxyglucose in human monocyte-macrophages in vitro. Eur J Nucl Med Mol Imaging 2003; 30: 267-273.

[19] Folco EJ, Sheikine Y, Rocha VZ, Christen T, Shvartz E, Sukhova GK, Di Carli MF and Libby P. Hypoxia but not inflammation augments glucose uptake in human macrophages: Implications for imaging atherosclerosis with 18-fluorine-labeled 2-deoxy-D-glucose positron emission tomography. J Am Coll Cardiol 2011; 58: 603-614.

[20] Figueroa AL, Subramanian SS, Cury RC, Truong QA, Gardecki JA, Tearney GJ, Hoffmann U, Brady TJ and Tawakol A. Distribution of inflammation within carotid atherosclerotic plaques with high-risk morphological features: a comparison between positron emission tomography activity, plaque morphology, and histopathology. Circ Cardiovasc Imaging 2012; 5: 69-77.

[21] Tawakol A, Migrino RQ, Bashian GG, Bedri S, Vermylen D, Cury RC, Yates D, LaMuraglia GM, Furie K, Houser S, Gewirtz H, Muller JE, Brady TJ and Fischman AJ. In vivo 18F-fluorodeoxyglucose positron emission tomography imaging provides a noninvasive measure of carotid plaque inflammation in patients. J Am Coll Cardiol 2006; 48: 1818-1824.

[22] Hag AM, Pedersen SF, Christoffersen C, Binderup T, Jensen MM, Jorgensen JT, Skovgaard D, Ripa RS and Kjaer A. (18)F-FDG PET imaging of murine atherosclerosis: association with gene expression of key molecular markers. PLoS One 2012; 7: e50908

[23] Ogawa M, Ishino S, Mukai T, Asano D, Teramoto N, Watabe H, Kudomi N, Shiomi M, Magata Y, Iida H and Saji H. (18)F-FDG accumulation in atherosclerotic plaques: immunohistochemical and PET imaging study. J Nucl Med 2004; 45: 1245-1250.

[24] Hyafil F, Cornily JC, Rudd JH, Machac J, Feldman LJ and Fayad ZA. Quantification of inflammation within rabbit atherosclerotic plaques using the macrophage-specific CT contrast agent N1177: a comparison with 18F-FDG PET/CT and histology. J Nucl Med 2009; 50: 959-965.

[25] Zhang Z, Machac J, Helft G, Worthley SG, Tang C, Zaman AG, Rodriguez OJ, Buchsbaum MS, Fuster V and Badimon JJ. Non-invasive imaging of atherosclerotic plaque macrophage in a rabbit model with F-18 FDG PET: a histopathological correlation. BMC Nucl Med 2006; 6: 3.

[26] von Schulthess GK, Steinert HC and Hany TF. Integrated PET/CT: current applications and future directions. Radiology 2006; 238: 405-422.

[27] Davies JR, Izquierdo-Garcia D, Rudd JH, Figg N, Richards HK, Bird JL, Aigbirhio FI, Davenport AP, Weissberg PL, Fryer TD and Warburton EA. FDG-PET can distinguish inflamed from non-inflamed plaque in an animal model of atherosclerosis. Int J Cardiovasc Imaging 2010; 26: 41-48.

[28] Soret M, Bacharach SL and Buvat I. Partial-volume effect in PET tumor imaging. J Nucl Med 2007; 48: 932-945.

[29] Adams MC, Turkington TG, Wilson JM and Wong TZ. A systematic review of the factors affecting accuracy of SUV measurements. AJR Am J Roentgenol 2010; 195: 310-320.

[30] Xiao YF, Wang B, Wang X, Du F, Benzinou M and Wang YX. Xylazine-induced reduction of tissue sensitivity to insulin leads to acute hyperglycemia in diabetic and normoglycemic monkeys. BMC Anesthesiol 2013; 13: 33.

[31] Hsu WH and Hummel SK. Xylazine-induced hyperglycemia in cattle: a possible involvement of alpha 2-adrenergic receptors regulating insulin release. Endocrinology 1981; 109: 825-829.

[32] Brown ET, Umino Y, Loi T, Solessio E and Barlow R. Anesthesia can cause sustained hyperglycemia in C57/BL6J mice. Vis Neurosci 2005; 22: 615-618.

[33] Bucerius J, Mani V, Moncrieff C, Machac J, Fuster V, Farkouh ME, Tawakol A, Rudd JH and Fayad ZA. Optimizing 18F-FDG PET/CT imaging of vessel wall inflammation: the impact of 18F-FDG circulation time, injected dose, uptake parameters, and fasting blood glucose levels. Eur J Nucl Med Mol Imaging 2014; 41: 369-383.

[34] Elkhawad M, Rudd JH, Sarov-Blat L, Cai G, Wells R, Davies LC, Collier DJ, Marber MS, Choudhury RP, Fayad ZA, Tawakol A, Gleeson FV, Lepore JJ, Davis B, Willette RN, Wilkinson IB, Sprecher DL and Cheriyan J. Effects of p38 mitogen-activated protein kinase inhibition on vascular and systemic inflammation in patients with atherosclerosis. JACC Cardiovasc Imaging 2012; 5: 911-922.

[35] Wu YW, Kao HL, Huang CL, Chen MF, Lin LY, Wang YC, Lin YH, Lin HJ, Tzen KY, Yen RF, Chi YC, Huang PJ and Yang WS. The effects of 3-month atorvastatin therapy on arterial inflammation, calcification, abdominal adipose tissue and circulating biomarkers. Eur J Nucl Med Mol Imaging 2012; 39: 399-407.